CHEMISTRY
A EUROPEAN JOURNAL

DOI: 10.1002/chem.200903195

Large Porphyrin Squares from the Self-Assembly of *meso*-Triazole-Appended L-Shaped *meso–meso*-Linked Zn^{II}–Triporphyrins: Synthesis and Efficient Energy Transfer

Chihiro Maeda,[a] Pyosang Kim,[b] Sung Cho,[b] Jong Kang Park,[b] Jong Min Lim,[b] Dongho Kim,*[b] Josh Vura-Weis,[c] Michael R. Wasielewski,*[c] Hiroshi Shinokubo,[d] and Atsuhiro Osuka*[a]

Abstract: *meso*-Triazolyl-appended Zn^{II}–porphyrins were readily prepared by Cu^{I}-catalyzed 1,3-dipolar cycloaddition of benzyl azide to *meso*-ethynylated Zn^{II}–porphyrin (click chemistry). In noncoordinating $CHCl_3$ solvent, spontaneous assembly occurred to form tetrameric array $(\mathbf{3})_2$ from *meso–meso*-linked diporphyrins **3**, and dodecameric porphyrin squares $(\mathbf{4})_4$ and $(\mathbf{5})_4$ from the L-shaped *meso–meso*-linked triporphyrins **4** and **5**. The structures of these assemblies were examined by ^{1}H NMR spectra, absorption spectra, and their gel permeation chromatography (GPC) retention time. Furthermore, the structures of the dodecameric porphyrin squares $(\mathbf{4})_4$ and $(\mathbf{5})_4$ were probed by small- and wide-angle X-ray scattering (SAXS/WAXS) measurements in solution using a synchrotron source. Excitation-energy migration processes in these assemblies were also investigated in detail by using both steady-state and time-resolved spectroscopic methods, which revealed efficient excited-energy transfer (EET) between the *meso–meso*-linked Zn^{II}–porphyrin units that occurred with time constants of 1.5 ps^{-1} for $(\mathbf{3})_2$ and 8.8 ps^{-1} for $(\mathbf{5})_4$.

Keywords: energy transfer · photosynthesis · porphyrinoids · self-assembly · triazoles

Introduction

In the photosynthetic antennae LH1 and LH2, efficient excitation-energy transfers (EET) among chlorophylls are crucially important for light-energy harvesting, which is realized by regularly arranged cyclic wheel-like structures.[1] Continuous efforts have been devoted to the synthesis and characterization of artificial photosynthetic systems that can mimic key features of EET in natural LHs.[2] Naturally, particular attention has been focused on the construction of cyclic porphyrin arrays[3] by means of a covalent[4,5] or noncovalent approach in view of their structural similarity to LH1 and LH2.[6–9] Covalent synthesis has the advantages of robust stability and precise control of the spatial arrangement. In addition, a proper choice of spacer also allows well-defined control of electronic interactions between constituent chromophores. However, as the size becomes larger, covalent synthesis becomes increasingly difficult and inefficient. As a more convenient but promising strategy, noncovalent, supramolecular assembly has emerged as an effective means for the construction of two- or three-dimensional architectures. The importance of this noncovalent strategy comes from the fact that the natural systems rely on noncovalent interac-

[a] C. Maeda, Prof. Dr. A. Osuka
Department of Chemistry, Graduate School of Science
Kyoto University, Sakyo-ku, Kyoto, 606-8502 (Japan)
Fax: (+81) 75-753-3970
E-mail: osuka@kuchem.kyoto-u.ac.jp

[b] P. Kim, S. Cho, J. K. Park, J. M. Lim, Prof. Dr. D. Kim
Center for Ultrafast Optical Characteristics Control and
Department of Chemistry
Yonsei University, Seoul, 120-749 (Korea)
Fax: (+2) 2-2123-2434
E-mail: dongho@yonsei.ac.kr

[c] J. Vura-Weis, Prof. Dr. M. R. Wasielewski
Department of Chemistry and
Argonne-Northwestern Solar Energy Research
(ANSER) Center, Northwestern University
Evanston IL, 60208-3113 (USA)
Fax: (+1) 847-467-1425
E-mail: m-wasielewski@northwestern.edu

[d] Prof. Dr. H. Shinokubo
Department of Applied Chemistry, Graduate School of Engineering
Nagoya University, Chikusa-ku, Nagoya 464-8603 (Japan)

Supporting information for this article is available on the WWW under http://dx.doi.org/10.1002/chem.200903195.

tions, as seen in LH1 and LH2 complexes. For such a noncovalent assembly, the coordination interaction between zinc(II)–porphyrin and pyridine[7,8] or imidazole[9] moieties has been particularly attractive because of its large association constant and favorable tendency not to spoil the photoexcited-state dynamics of porphyrins.[10] Here it is worth noting that the syntheses of porphyrins that bear pyridine or imidazole are not trivial, since the usual porphyrin synthesis on the basis of acid-catalyzed condensation is severely hampered by such a coordinating basic moiety. In this context, we recently demonstrated the utility of so-called "click chemistry" that used a Cu^{I}-catalyzed 1,3-dipolar cycloaddition reaction of benzyl azide to *meso*-ethynyl-substituted porphyrins for the preparation of *meso*-1,2,3-triazole-substituted porphyrins (Scheme 1).[11,12] Actually, the synthesis of triazolyl-appended Zn^{II}–porphyrin **1** was quite facile; it formed a face-to-face dimer, $(\mathbf{1})_2$, with an association constant of $10^5\,M^{-1}$. The association constant of the dimer was dramatically increased by implementing additional hydrogen-bonding interactions, as demonstrated by the dimerization to form $(\mathbf{2})_2$ with an association constant larger than $10^{11}\,M^{-1}$.[11b] In the latter case, the most stable assembly $(\mathbf{2})_2$ was chosen from three possible atropisomeric face-to-face dimers with respect to the position of the ester group. Then it was suggested that the relatively small coordination ability of triazole, as compared with the corresponding association constants of the similar face-to-face diporphyrins pyridine ($\approx 10^8\,M^{-1}$)[7b] and imidazole ($\approx 10^{11}\,M^{-1}$)[6f] could be suitable for more precise recognition through multiple dynamic intermolecular interactions.

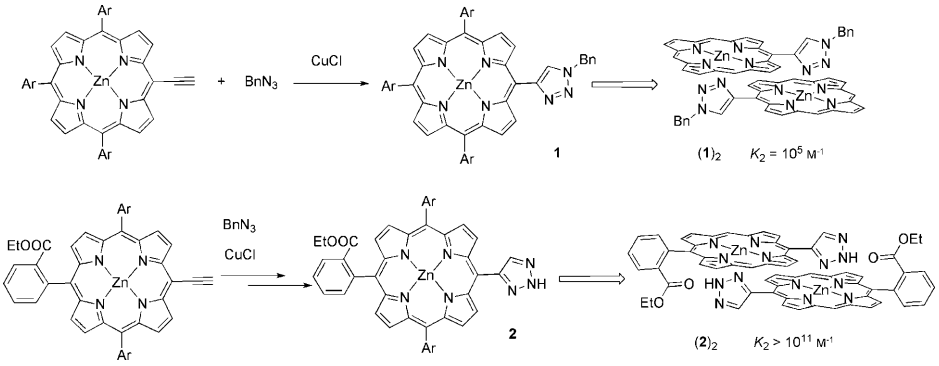

Scheme 1. Syntheses of **1** and **2** and their self-assembling to $(\mathbf{1})_2$ and $(\mathbf{2})_2$. Ar = 3,5-di-*tert*-butylphenyl.

In this paper, 1,2,3-triazole rings were introduced at the *meso* positions of *meso–meso*-linked diporphyrin and triporphyrin[13] to provide **3**, **4**, and **5** with the aim of forming larger but well-ordered assemblies by multiple coordination bonds. Actually, spontaneous self-assembly occurred to form porphyrin box $(\mathbf{3})_2$ from **3**, and large porphyrin squares $(\mathbf{4})_4$ and $(\mathbf{5})_4$ from **4** and **5** by complementary triazole–zinc(II) coordinative interactions. These assemblies displayed larger absorption spectral coverage due to exciton coupling and efficient intra-assembly EET that has been confirmed by ultra-fast time-resolved measurements.

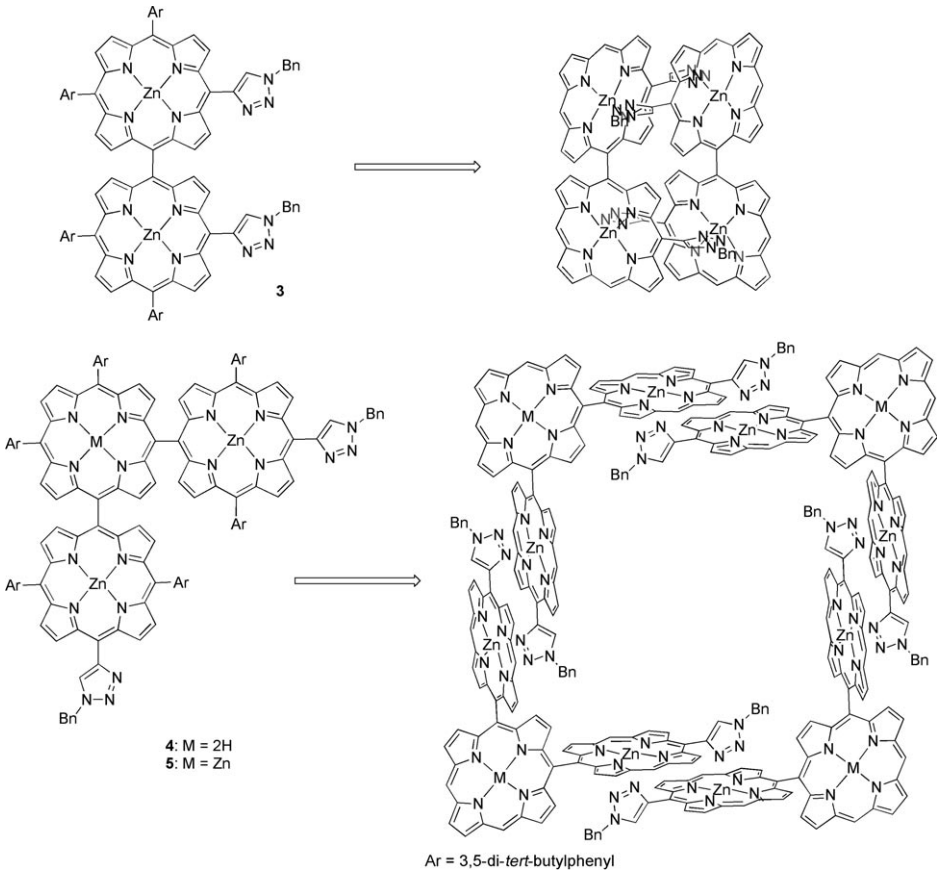

Results

Synthesis: The syntheses and self-assembly behaviors of **1** and **2** were reported previously.[11] Synthetic routes to **3**, **4**,

and **5** are illustrated in Scheme 2. Ethynyl groups were introduced to *meso–meso*-linked Zn^{II}–diporphyrin **6** by bromination with *N*-bromosuccinimide (NBS), subsequent Sonogashira coupling reaction with trimethylsilylacetylene, and final deprotection of the trimethylsilyl group with tetrabutylammonium fluoride (TBAF). A click reaction of 5,5′-diethynyl-substituted *meso–meso*-linked Zn^{II}–diporphyrin **7** with benzyl azide gave 5,5′-bistriazolyl Zn^{II}–diporphyrin **3** in 61% yield. The synthesis of **4** and **5** was performed as follows. Triazole-appended Zn^{II}–porphyrin **9** was prepared by the 1,3-dipolar cycloaddition of benzyl azide to *meso*-ethynylated Zn^{II}–porphyrin **8**. 5-Borylated-15-triazolyl-substituted Zn^{II}–porphyrin **10** was prepared from **9** by means of *meso*-selective NBS bromination followed by Pd-catalyzed borylation. A Suzuki–Miyaura coupling reaction[14] of 5,10-dibromo-substituted porphyrin **11** and **10** furnished Zn^{II} free-base hybrid triporphyrin **4** in 24% yield, which was converted into Zn^{II}–porphyrin trimer **5** by metalation with $Zn(OAc)_2$ in 85% yield.

Characterization: The ^{1}H NMR spectrum of **3** in $CDCl_3$ exhibits a single set of signals with clear upfield shifts for the β protons at $\delta = 6.3$ and 6.2 ppm, thereby indicating the formation of a discrete face-to-face dimer, $(\mathbf{3})_2$. The ^{1}H NMR spectrum of **4** in $CDCl_3$ exhibits two sets of signals with normal chemical shifts and upfield-shifted chemical shifts for the β protons ($\delta = 5.8$ and 5.5 ppm) in a ratio of 1:2, thereby suggesting the formation of the expected tetrameric porphyrin square. Actually, these two sets of peaks are considered to correspond to the corner four free-base porphyrins and the four side-positioning face-to-face Zn^{II} dimeric pairs in a ratio of 1:2, since the signals due to the latter parts are observed in the range of a high-field-shifted region. In [D_5]pyridine, these porphyrin oligomers **3**, **4**, and **5** exhibit simple ^{1}H NMR spectra, thereby indicating their monomeric nature (see the Supporting Information).

The molecular size of these aggregates was examined by analytical GPC-HPLC (Figure 1). The GPC retention time was distinctly shorter with $CHCl_3$ than with coordinating THF as eluent, thereby indicating that assembly formation occurs in $CHCl_3$ but not in THF. It is worthy of note that these porphyrins formed assemblies under highly diluted conditions in $CHCl_3$. Importantly, the retention times exhibited a good correlation with increasing molecular weights of $(\mathbf{2})_2$, $(\mathbf{3})_2$, $(\mathbf{4})_4$, and $(\mathbf{5})_4$ (Table 1 and Figure 2), which were slightly longer than those of the polystyrene standards that were roughly linear in spite of their propensity to take coiled conformations.

The structures of aggregates $(\mathbf{4})_4$ and $(\mathbf{5})_4$ were also studied by small- and wide-angle X-ray scattering (SAXS/WAXS) measurements performed on their 10^{-4} M solutions in toluene using a high-flux synchrotron

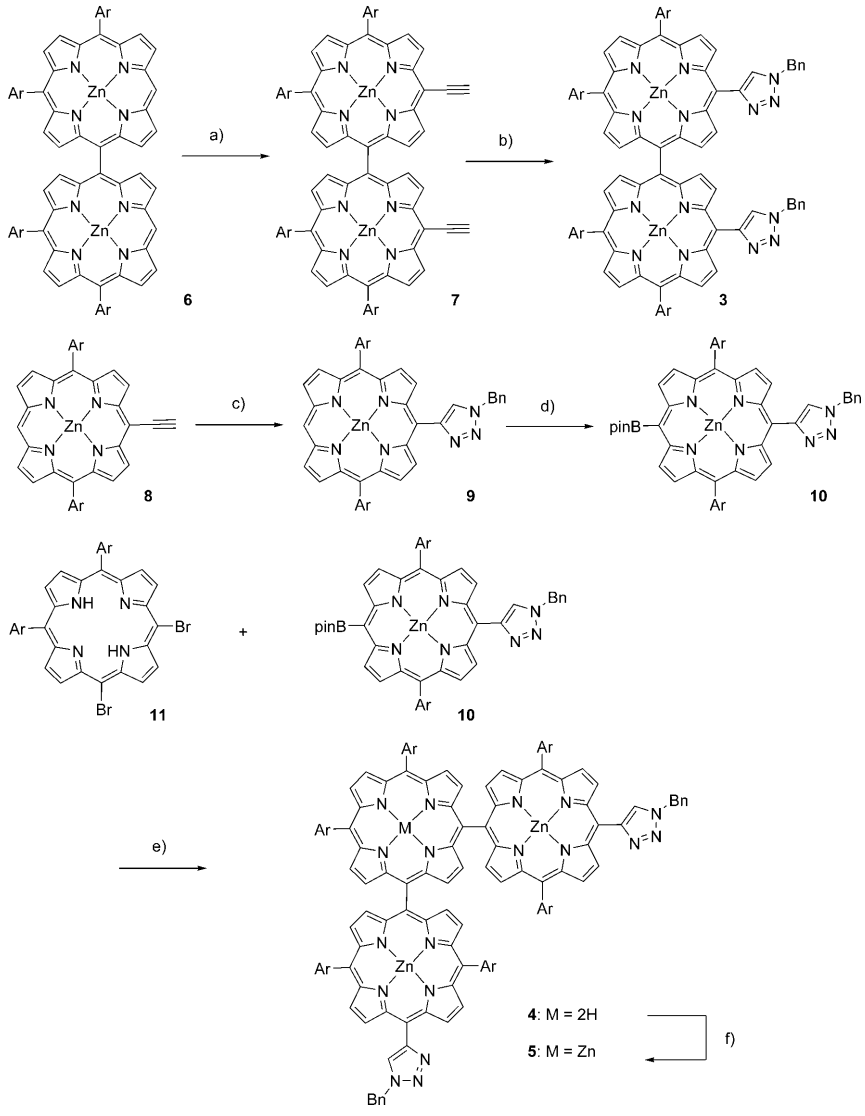

Scheme 2. a) 1) NBS, $CHCl_3$, pyridine, 0°C; 2) trimethylsilylacetylene, CuI, $[PdCl_2(PPh_3)_2]$, THF, Et_3N, RT; 3) TBAF, $CHCl_3$, RT, 52%. b) BnN_3, CuCl, toluene, 100°C, 61%. c) BnN_3, CuCl, toluene, 100°C, 74%. d) NBS, $CHCl_3$, pyridine, 0°C, then HBpin, $[PdCl_2(PPh_3)_2]$, Et_3N, dioxane, reflux, 91%. e) $[Pd_2(dba)_3]$ (dba = dibenzylideneacetone), tri-2-furylphosphine, Cs_2CO_3, CsF, dioxane, DMF, reflux, 24%. f) $Zn(OAc)_2$, $CHCl_3$, MeOH, RT, 85%. Ar = 3,5-di-*tert*-butylphenyl.

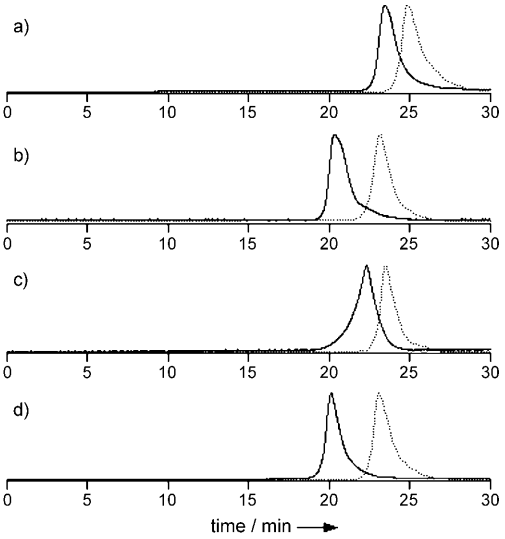

Figure 1. Analytical GPC-HPLC chromatograms of a) **2**, b) **3**, c) **4**, and d) **5** eluted with $CHCl_3$ (solid line) and with THF (dashed line).

Table 1. Calculated molecular weights and GPC-HPLC retention times.

Compound	Molecular formula	M_{calcd}	t [min]
2	$C_{59}H_{61}N_7O_2Zn$	965.6	25.0
$(\mathbf{2})_2$	$C_{118}H_{122}N_{14}O_4Zn_2$	1931.1	23.4
3	$C_{114}H_{116}N_{14}Zn_2$	1813.1	23.5
$(\mathbf{3})_2$	$C_{228}H_{232}N_{28}Zn_4$	3626.1	22.3
4	$C_{162}H_{168}N_{18}Zn_2$	2498.0	23.2
$(\mathbf{4})_4$	$C_{648}H_{672}N_{72}Zn_8$	9992.0	20.3
5	$C_{162}H_{166}N_{18}Zn_3$	2561.4	23.1
$(\mathbf{5})_4$	$C_{648}H_{664}N_{72}Zn_{12}$	10245.6	20.1

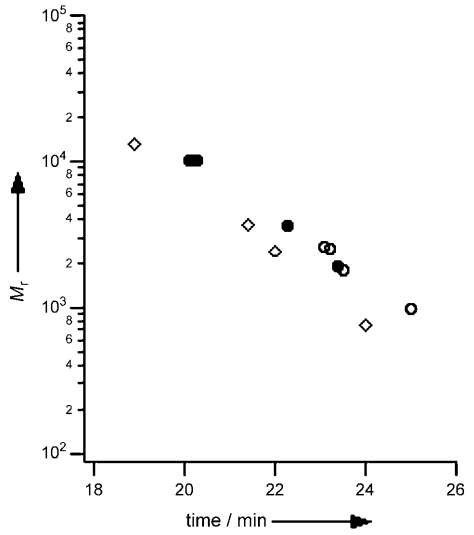

Figure 2. Relationship of the retention time versus molecular weight (●: aggregated structures; ○: dissociated structures; ◇: polystyrene standard).

source (Advanced Photon Source at Argonne National Laboratory). The solution-phase scattering pattern for $(\mathbf{5})_4$ was obtained for the q region ($0.01 < q < 1.0$ Å^{-1}; Figure 3a). In the low-resolution scattering region ($q < 0.1$ Å^{-1}), the scattering intensity follows the Guinier relationship, $I(q) = I(0)\exp(-q^2R_g^2/3)$, which is parameterized in terms of the forward scattering amplitude, $I(0)$, and the radius of gyration, R_g.[15] The linearity of the Guinier plot between $0.001 < q^2 < 1.0$ Å^{-2} (Figure 3b) indicated that the sample consisted of a monodisperse structure.[16] The least-squares fit to the linear data reveals a radius of gyration of 18.1 Å. The monodisperse nature of $(\mathbf{5})_4$ in toluene allowed direct comparisons between reciprocal-space scattering patterns and real-space molecular models through atomic-pair distribution function (PDF) analysis. The experimental PDF for $(\mathbf{5})_4$ in toluene was obtained using the X-ray scattering fitting program GNOM (Figure 3c).[17] The peaks in the PDF at 23.5 Å were the result of atomic pair correlations between the side-to-side pairs.[18] Optimized models of $(\mathbf{5})_4$ revealed an average Zn–Zn distance of 23.1 Å for the analogous pair correlations. For $(\mathbf{4})_4$ the theoretical values of R_g calculated by the PDF were 16.2 Å for the experiment, which were a very good match with the R_g value of 15.5 Å for model (Figure S11 in the Supporting Information).[19] The PDF obtained from monomeric model showed entirely different peaks.

Steady-state absorption, fluorescence, and fluorescence excitation anisotropy: In the present study, we used $CHCl_3$ and pyridine as solvents, in which the triazole-appended porphyrins exist as aggregates and monomers, respectively. Figure 4 shows the absorption spectra of **2**, **3**, and **5** in $CHCl_3$ and pyridine. As reported previously, the absorption spectrum of **2** in pyridine exhibited a sharp Soret band at 433 nm, which was typical of a monomeric Zn^{II}–porphyrin, whereas that in $CHCl_3$ displayed a blueshifted and split Soret band that was characteristic of face-to-face dimers, thus indicating the formation of $(\mathbf{2})_2$.[9a,11b] The absorption spectrum of **3** in pyridine featured a split Soret band at 430 and 469 nm characteristic of *meso–meso*-linked Zn^{II}–diporphyrin, and that in $CHCl_3$ exhibited a narrowly split Soret band that is characteristic of a porphyrin box that consists of two complementary coordinating *meso–meso*-linked Zn^{II}–diporphyrins,[8a,b] thus indicating the monomeric dissociation in pyridine and the formation of dimeric assembly $(\mathbf{3})_2$ in $CHCl_3$, respectively. The absorption spectrum of **5** in pyridine was quite similar to that of L-shaped *meso–meso*-linked Zn^{II}–triporphyrin,[14b,c] whereas that in $CHCl_3$ was more broad and complicated in line with the formation of $(\mathbf{5})_4$. The absorption spectrum of **5** in $CHCl_3$ will be discussed later.

The S_1 fluorescence spectra of **2**, **3**, and **5** in pyridine were observed with gradually redshifted peaks at 613, 641, and 646 nm. Compared with these spectra, the fluorescence spectra of assemblies $(\mathbf{2})_2$, $(\mathbf{3})_2$, and $(\mathbf{5})_4$ in $CHCl_3$ become slightly blueshifted and sharpened (Figure 4). Observed changes in the fluorescence spectra of **3** and $(\mathbf{3})_2$ are noteworthy in that the vibronic structure is clearly restored in the latter. This can be explained in terms of considerable rigidification of the dihedral angle in the *meso–meso*-linked

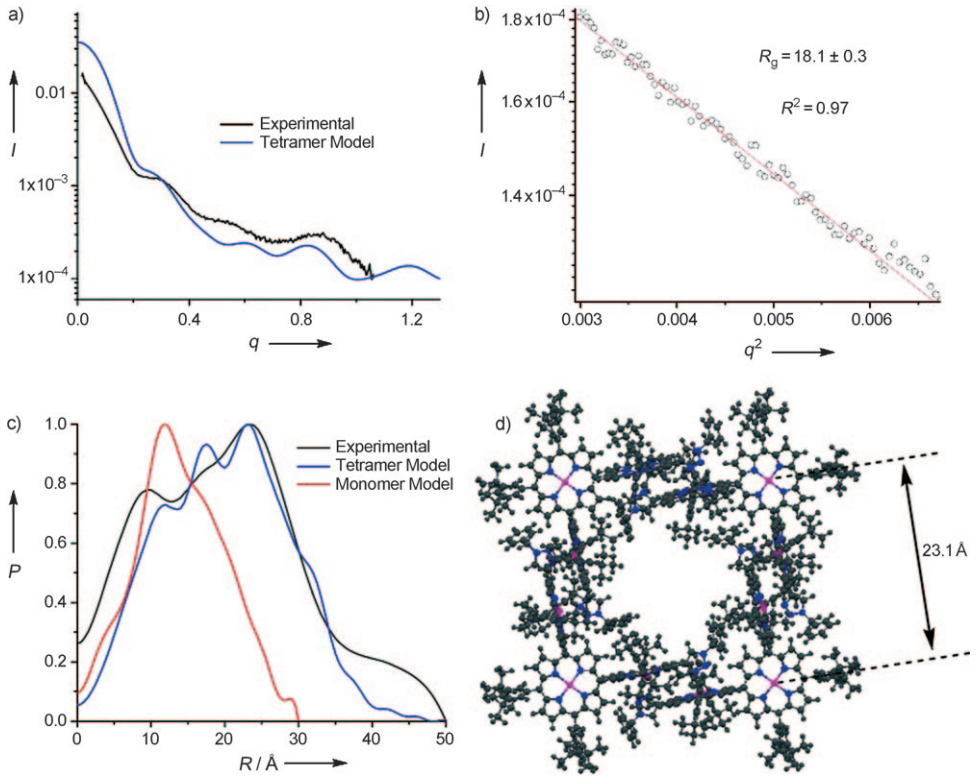

Figure 3. a) Experimental scattering intensity, $I(q)$, versus scattering length vector, q, data for a solution of **5** in toluene (4.7×10^{-4} M; $0.1<q<1.0$ Å^{-1} region). b) Scattering intensity versus q^2 for the same sample ($0.001<q^2<0.01$ Å^{-2} region). Guinier fit to the data is also shown. c) Atomic pair distribution functions (PDFs) for **5** in toluene obtained using the program GNOM. d) Optimized structure of $(\mathbf{5})_4$.

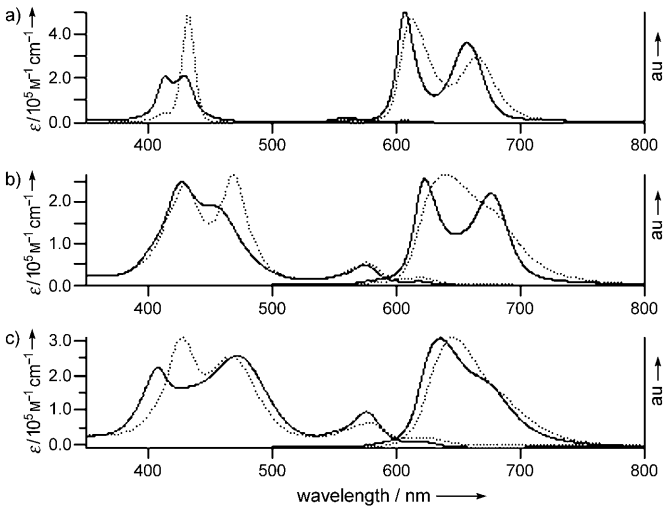

Figure 4. Steady-state absorption (left) and fluorescence (right) spectra of a) **2**, b) **3**, and c) **5** in $CHCl_3$ (solid line) and pyridine (dotted line).

diporphyrins due to the formation of the self-assembled complex. In the case of $(\mathbf{5})_4$, however, the fluorescence spectral changes from that of **5** are only marginal because of the greater conformational flexibility of $(\mathbf{5})_4$. In addition, the Stokes shifts are commonly smaller in the aggregates $(\mathbf{2})_2$, $(\mathbf{3})_2$, and $(\mathbf{5})_4$, than monomeric **2**, **3**, and **5**, respectively, thereby suggesting that the self-assembling leads to more rigid conformation.

The steady-state fluorescence excitation anisotropy spectra were measured for **2**–**5** and $(\mathbf{2})_2$–$(\mathbf{5})_4$ and are compared in Figure 5. The polarization anisotropy measurement reveals the relative orientation of emissive transition dipole moment with respect to that of excitation, which changes through depolarization channels such as molecular rotational motion and excitation-energy transfer. Whereas **2** and **3** displayed anisotropy profiles that exhibited negative anisotropy in the high-energy Soret band and positive anisotropies in the low-energy Soret and Q bands, **5** showed a distinct feature: relatively decreased anisotropy in the low-energy Soret band and Q bands in spite of a larger molecular volume that caused slower rotational diffusion time. A reason for this feature may be a new depolarization channel in **5**, which is expected to be similar to the energy-transfer process observed in the directly *meso*–*meso*-linked porphyrin rings through the bidirectional coupling with the nearest neighboring porphyrins.[5b] In $(\mathbf{3})_2$, an abrupt decrease in the anisotropy value was observed in the entire spectral region as compared with **3**, thereby suggesting the occurrence of intracomplex fast energy-transfer processes. In contrast to $(\mathbf{3})_2$, $(\mathbf{5})_4$ exhibited an increase in the anisotropy value in the low-energy Soret and Q bands compared with that of **5**. Since $(\mathbf{5})_4$ should have the same depolarization channel as that of **5**, the observed increase in the anisotropy value for $(\mathbf{5})_4$ was considered due to its much slower rotational diffusion process.

Fluorescence decay measurements: The time-resolved fluorescence decays of **2**–**5** and $(\mathbf{2})_2$–$(\mathbf{5})_4$ were measured and their fitted fluorescence lifetimes are tabulated in Table 2. Importantly, all the models retain relatively long fluorescence lifetimes (>1.45 ns), which is an important requirement for artificial photosynthetic antenna models. Their fluorescence decay profiles exhibit monoexponential behaviors, and the overall fluorescence lifetimes are gradually reduced in going from **2**–**5** to $(\mathbf{2})_2$–$(\mathbf{5})_4$ and also in the order of $\mathbf{2}>\mathbf{3}>\mathbf{5}$ as well as $(\mathbf{2})_2>(\mathbf{3})_2>(\mathbf{5})_4$. These decreased fluorescence lifetimes may be ascribed to increased conformational heterogeneity associated with an increase in molecular size.

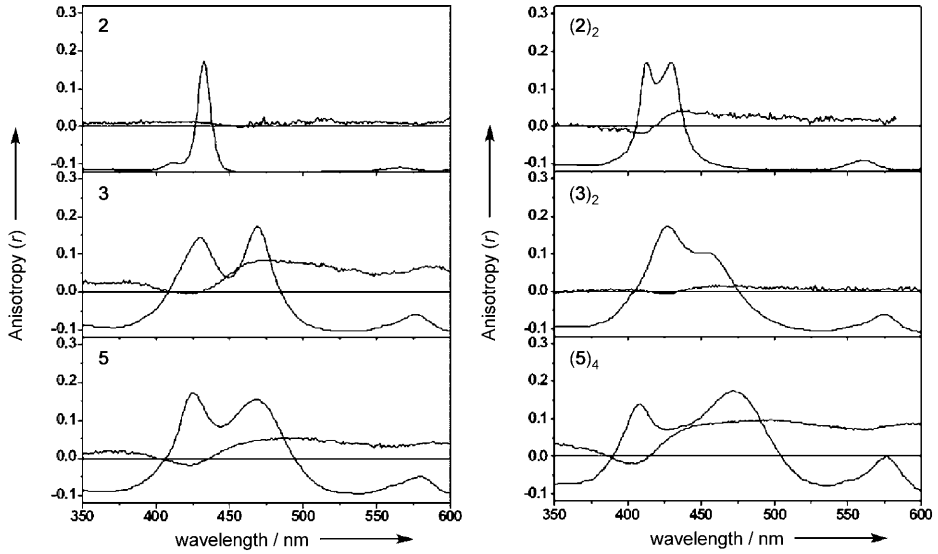

Figure 5. Steady-state fluorescence excitation anisotropy spectra of **2**, **3**, and **5** in pyridine (left) and $CHCl_3$ (right). The spectra were obtained using parallel and perpendicular orientation between excitation and emission polarization at a fixed emission wavelength of 610 nm.

Table 2. Photophysical parameters for **2**–**5** and $(\mathbf{2})_2$–$(\mathbf{5})_4$.

Sample	Solvent	λ_A [nm]	λ_F [nm]	Φ_F[a]	τ [ns]	k_r [10^7 s^{-1}]	k_{nr} [10^8 s^{-1}]	Φ[b] [ns]
2	pyridine	433, 566, 607	613	0.035	2.04	1.72	4.85	0.44 ± 0.05
$(\mathbf{2})_2$	$CHCl_3$	414, 430, 561, 605	607	0.020	1.88	1.06	5.19	0.64 ± 0.14
3	pyridine	430, 469, 576, 618	641	0.058	1.90	3.05	4.95	1.07 ± 0.34
$(\mathbf{3})_2$	$CHCl_3$	428, 452, 575, 618	623	0.023	1.58	1.46	6.20	–
5	pyridine	428, 468, 579, 625	646	0.068	1.86	3.66	5.01	1.78 ± 0.16
$(\mathbf{5})_4$	$CHCl_3$	408, 473, 576, 620	636	0.040	1.45	2.76	6.62	4.01 ± 2.07

[a] Quantum yield was determined with reference to the value (0.033) of zinc(II) tetraphenylporphyrin in toluene. [b] The rotational diffusion time; see the Supporting Information.

To quantitatively analyze the characteristics of the S_1 state, we calculated the radiative and nonradiative decay rates using the fluorescence quantum yields and the S_1 fluorescence lifetimes. Consequently, the increase of fluorescence quantum yields in going from **2** to **5** and $(\mathbf{2})_2$ to $(\mathbf{5})_4$ is mainly caused by the increase of radiative decay rates, which give information about the difference in excitonic coupling strength through the arrangement of transition dipole moments that lead to a change in radiative decay rates. Interestingly, the extent of increase in the radiative decay rates has a different pattern between **2**–**5** and $(\mathbf{2})_2$–$(\mathbf{5})_4$; the radiative rate is increased by 77% for **3** and 112% for **5** as compared with **2** but the increase is 38 and 160% for $(\mathbf{3})_2$ and $(\mathbf{5})_4$, respectively, as compared with $(\mathbf{2})_2$. In spite of the same bidirectional arrangements of transition dipole moments, $(\mathbf{5})_4$ has a larger increase (160%) than the case of **5** (112%), mainly because of additional linear arrangements of transition dipole moments by the formation of a square-type self-assembled complex. Additionally, the reason for the small increase (38%) in $(\mathbf{3})_2$ relative to **3** is probably due to competition of H- and J-type coupling among the transition dipole moments along the long axes by the self-assembling geometry, thus leading to the reduced transition dipole moment.

Intensity-dependent femtosecond transient absorption (TA) decay: To explore the excitation-energy-transfer processes, the pump-power dependencies of the femtosecond transient absorption measurements were examined for $(\mathbf{2})_2$–$(\mathbf{5})_4$ using **2**–**5** as reference molecules with Q-band excitation at 570 nm (Table 3, Figure 6). Monomeric species **2**–**5** and the dimeric assembly $(\mathbf{2})_2$ revealed no pump-power-dependent TA decays that were in agreement with the S_1 state lifetimes measured by time-correlated single-photon counting (TCSPC) techniques. On the other hand, $(\mathbf{3})_2$ and $(\mathbf{5})_4$ showed fast decay components τ_1 (1.5 ps) and τ_2 (7.5 ps), respectively, the amplitudes of which are sensitive to the photoexcitation intensity as compared to the S_1 state lifetime. The pump-power dependence on the TA decay is a strong indication of singlet–singlet annihilation processes, because the intense excitation or high density of photons generates two or more excitons within one self-assembled complex, and then the recombination process between excitons leads to a fast deactivation process. Because the TA decays of **3** and **5** showed no intensity dependence, the observed singlet–singlet annihilation times in $(\mathbf{3})_2$ and $(\mathbf{5})_4$ suggested that the exciton–exciton recombination processes occur in these assem-

Table 3. Pump-power-dependent transient absorption decay parameters for $(\mathbf{2})_2$, $(\mathbf{3})_2$, and $(\mathbf{5})_4$

	Pump power [μW]	Fitted decay times [ps]		
		τ_1	τ_2	τ_3
$(\mathbf{2})_2$	520	2000 (100%)		
	446	2000 (100%)		
	360	2000 (100%)		
$(\mathbf{3})_2$	520	1.5 (18%)	1640 (82%)	
	446	1.5 (8%)	1640 (92%)	
	360	–	1640 (100%)	
$(\mathbf{5})_4$	520	1.5 (30%)	7.5 (26%)	1510 (44%)
	446	1.8 (36%)	7.5 (15%)	1510 (49%)
	360	1.8 (24%)	7.5 (≈2%)	1510 (74%)

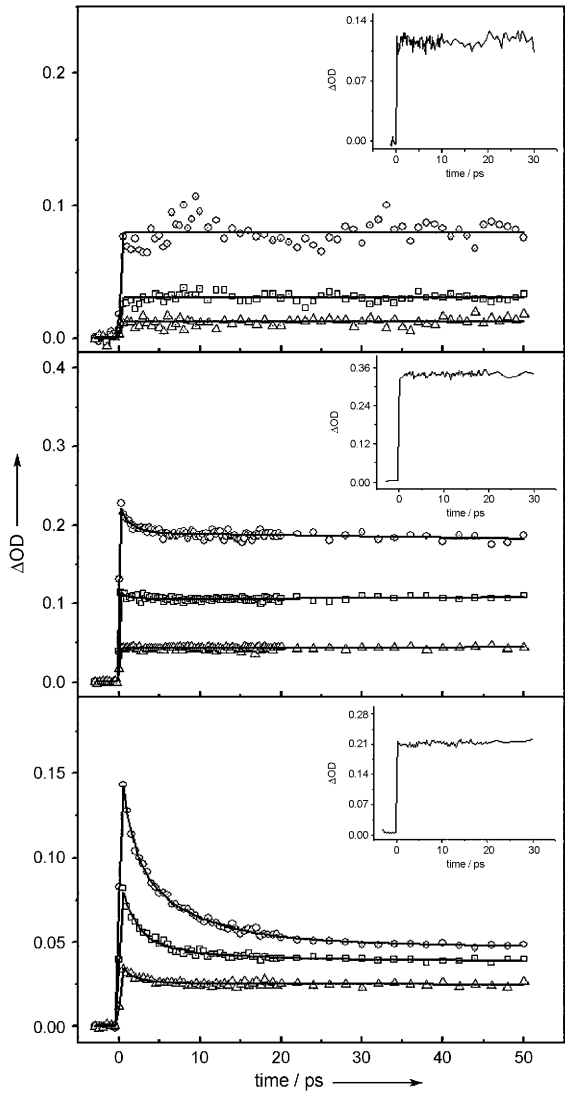

Figure 6. Power-dependent transient absorption decay profiles of $(\mathbf{2})_2$ (top), $(\mathbf{3})_2$ (middle), and $(\mathbf{5})_4$ (bottom) (○: 520 mW; □: 446 μW; △: 360 μW). The transient absorption decay profiles (520 μW) of **2**, **3**, and **5** is inserted. In the experiments, the pump and probe wavelengths were 570 and 520 nm, which are the Q-band excitation and induced absorption probe, respectively. The solvent used was toluene.

blies. The faster τ_1 (1.5–1.8 ps) component in the TA decay profile of $(\mathbf{5})_4$ might be associated with high-order annihilation processes, which could occur in multichromophoric systems, especially when the samples are excited by higher pump-power pulses. In addition, according to descriptions of the natural light-harvesting systems (LH1 and LH2), the singlet–singlet annihilation process is directly indicative of Förster-type incoherent energy transfer from the excited donor to an adjacent excited acceptor, thereby resulting in the formation of a doubly excited state that quickly relaxes to the singly excited state. Thus, the singlet–singlet annihilation process reflects the excitation-energy-transfer processes that occur in multichromophoric molecular assemblies such as $(\mathbf{2})_2$–$(\mathbf{5})_4$ in the present work.[20,21]

Discussion

The absorption spectral features of $(\mathbf{2})_2$, $(\mathbf{3})_2$, and $(\mathbf{5})_4$ can be explained in terms of the excitonic coupling theory (Figure 7). The Soret band of porphyrin monomer **2** has two perpendicular transition dipole moments $\boldsymbol{B}_x$ and $\boldsymbol{B}_y$ that are degenerate. In cofacial diporphyrin $(\mathbf{2})_2$, two transition dipole moments $\boldsymbol{B}_{x1}$ and $\boldsymbol{B}_{x2}$ are coupled as an H-type interaction, thus giving rise to a blueshifted band (high-energy Soret band), whereas $\boldsymbol{B}_{y1}$ and $\boldsymbol{B}_{y2}$ are considered to be coupled as a J-type interaction. Fortunately, we have determined the crystal structure of $(\mathbf{2})_2$,[11b] which is shown in Figure 8; the arrangement of the transition dipole moments is also indicated. This explains the absorption spectrum of $(\mathbf{2})_2$ nicely since the angle between $\boldsymbol{B}_{y1}$ and $\boldsymbol{B}_{y2}$ is 32.5°, which is characteristic for J-type interaction.[22] This geometry serves as an important structural motif in the exciton coupling of $(\mathbf{3})_2$ and $(\mathbf{5})_4$. In the case of *meso–meso*-linked diporphyrin **3**, the Soret band is split to a redshifted band and the original band because two dipole moments $\boldsymbol{B}_x$ along with the *meso–meso*-linked axis are strongly coupled as J-type interactions, but the coupling between $\boldsymbol{B}_{y1}$ and $\boldsymbol{B}_{z1}$ is negligible due to the perpendicular orientation. In assembly $(\mathbf{3})_2$, $\boldsymbol{B}_{y1}$, $\boldsymbol{B}_{y2}$ and $\boldsymbol{B}_{z1}$, $\boldsymbol{B}_{z2}$ are coupled in a similar manner to the low-energy Soret band of $(\mathbf{2})_2$, but the remaining four transition dipole moments $\boldsymbol{B}_x$ that are already J-type-coupled undergo additional H-type interaction to give rise to a blueshifted low-energy Soret band that is lower in energy than that of **3** (Figure 7). As reported previously,[14b] L-shaped triporphyrin **5** shows a split Soret band, the splitting width of which is close to those of *meso--meso*-linked diporphyrins such as **3**. But in $(\mathbf{5})_4$, the low-energy Soret band is further redshifted because of the additional exciton coupling with two transition dipole moments $\boldsymbol{B}_{x2}$ and $\boldsymbol{B}_{y2}$. For $\boldsymbol{B}_z$ components, the H-type interaction and out-of-plane arrangement of transition dipole moments create a high-energy Soret band that is distinctly observed at 408 nm [Eq. (1), Figure 7].

$$\tau_a = \frac{\tau_h}{8\sin^2(\pi/2N)} \quad (1)$$

The observed exciton–exciton annihilation process is closely associated with the excitation-energy-hopping process. Equation (1) correlates the annihilation time (τ_a) and the energy-hopping time (τ_h) for a one-dimensional cyclic multichromophoric system with N hopping units. Although $(\mathbf{5})_4$ contains 12 porphyrin monomer units, the number of hopping sites (N) is considered to be 4, that is, four of **5**. Because it is conceived that the excitation-energy transfer within approximately 200 fs occurs between *meso–meso* directly linked porphyrin monomers in the **5** moiety, we can directly assign the slowest annihilation time component as the energy-hopping time between four **5** units.[5,23] Therefore, using the observed annihilation time τ_2 in Table 3, the energy-hopping time τ_h of $(\mathbf{5})_4$ was evaluated to be 8.8 ps (Figure 9). This method of determining the energy-hopping

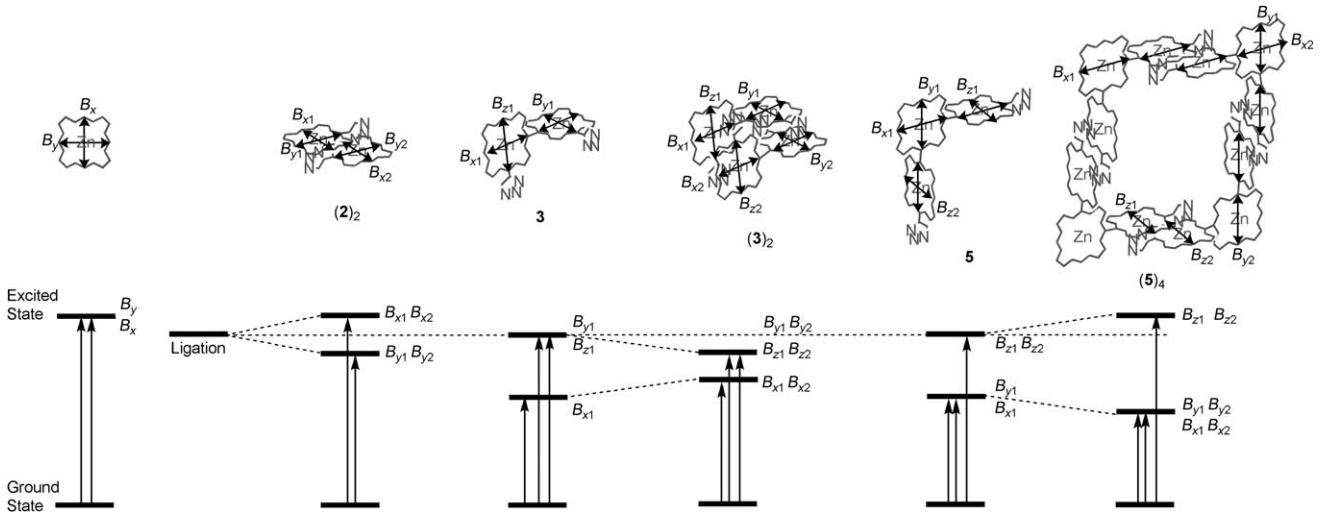

Figure 7. Exciton coupling in the assemblies

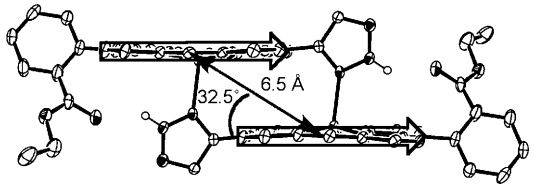

Figure 8. Crystal structure and schematic representation of dipole moments of $(\mathbf{2})_2$.

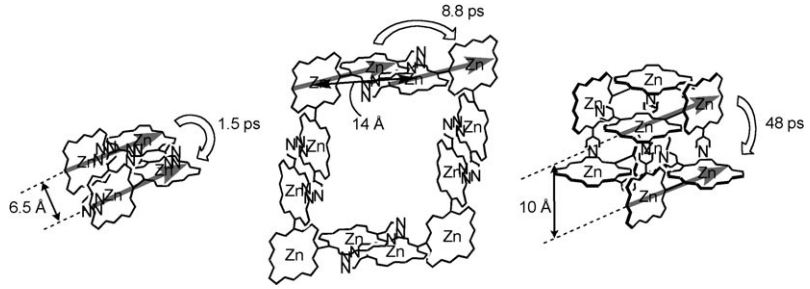

Figure 9. Schematic representation of energy hopping in the assemblies.

rate is also applicable to $(\mathbf{3})_2$, thereby resulting in an energy-hopping time of 1.5 ps between Zn^{II}–porphyrin units. In the case of $(\mathbf{3})_2$, the annihilation time represents directly the energy-hopping time because it has only two energy-hopping sites.

To confirm the energy-hopping model (Figure 9), the Förster-type energy-transfer rate was calculated by using Equation (2).[23,24]

$$K_T(r) = \frac{Q_D \kappa^2}{\tau_D r^6}\left(\frac{90000(\ln 10)}{128\pi^5 N n^4}\right)\int_0^\infty F_D(\lambda)\varepsilon_A(\lambda)\lambda^4 d\lambda \qquad (2)$$

in which κ^2 is the orientation factor, Q_D is the fluorescence quantum yield of the donor in the absence of acceptor, n is the refractive index of the medium, N is Avogadro's number, r is the distance between donor and acceptor, τ_D is the lifetime of the donor in the absence of acceptor, $F_D(\lambda)$ is the corrected fluorescence intensity of the donor normalized to unity, and $\varepsilon_A(\lambda)$ is the extinction coefficient of the acceptor at λ, which is typically measured in $M^{-1}cm^{-1}$. The distance r between neighboring and next-nearest-neighboring molecules in $(\mathbf{3})_2$ and $(\mathbf{5})_4$ are determined from the Soret-band excitonic dipole coupling and Q-band shift. In other words, **5** and **3** have the similar peak positions of low-energy Soret bands as well as Q bands, thereby indicating that we can assume the same transition dipole moments for the hopping units as that of **3**. This assumption results in the calculated distance of approximately 6.5 Å for $(\mathbf{3})_2$ and approximately 14 Å for $(\mathbf{5})_4$ (Figure 9). Using these values and κ^2 of 1 and 1.96 for $(\mathbf{3})_2$ and $(\mathbf{5})_4$, respectively, the Förster-type energy-transfer rates were calculated to be $(\approx 0.71\ ps)^{-1}$ and $(\approx 9.5\ ps)^{-1}$, which are in good agreement with the experimental hopping times. Therefore, although $(\mathbf{3})_2$ and $(\mathbf{5})_4$ are very closely spaced, we demonstrate that the experimental and calculated Förster-type energy-transfer rates confirm the schematic dipole–dipole interactions in $(\mathbf{3})_2$ and $(\mathbf{5})_4$ through the formation of self-assembled complexes (Figure 9).

Assemblies $(\mathbf{3})_2$ and $(\mathbf{5})_4$ show excitation-energy-hopping rates of $(1.5\ ps)^{-1}$ and $(8.8\ ps)^{-1}$ respectively. In particular, if we consider that the Förster energy-transfer rate is proportional to $1/r^6$, the $(\mathbf{5})_4$ complex shows a faster excitation-energy-hopping rate ($\approx$14 Å, $8.8\ ps^{-1}$) than $(\mathbf{3})_2$ ($\approx$6.5 Å,

1.5 ps^{-1}) or the previously reported porphyrin box (≈10 Å, 48 ps^{-1}).[8b] In the case of $(\mathbf{3})_2$, if we consider that the Förster energy-transfer rate is proportional to $1/r^6$, the energy-transfer rate of $(\mathbf{5})_4$ (≈14 Å) is expected to be approximately 150 ps^{-1} as compared with that of $(\mathbf{3})_2$, thereby resulting in a rate around 17 times slower than that of $(\mathbf{5})_4$. In the porphyrin box, when the distance between energy-hopping units is simply considered, the porphyrin box with the center-to-center distance of approximately 10 Å between energy-hopping units shows an excitation-energy-hopping rate around 5 times slower than that of $(\mathbf{5})_4$ although the distance between hopping units is larger by around 4 Å. This result may come from the competition between H- and J-type coupling of the transition dipole moments along the *meso–meso* linkage in $(\mathbf{3})_2$ or the porphyrin box and the parallel arrangement of transition dipole moments, thereby leading to much-decreased energy-transfer rates. On the contrary, the orientations between the transition dipole moments of **5** in $(\mathbf{5})_4$ are parallel to each other by the formation of square-type self-assembled complexes.

Conclusion

In this work, we have investigated the synthesis, self-assembly, and excitation-energy-hopping processes that occurs in self-assembled porphyrin array systems $(\mathbf{3})_2$ and $(\mathbf{5})_4$ constructed from 1,2,3-triazole-appended Zn^{II}–porphyrins **3** and **5**. The structures of these assemblies have been examined by their ^{1}H NMR, UV/Vis absorption spectroscopy; GPC retention time; and SAXS/WAXS measurements. The exciton–exciton annihilation process evidently represents the excitation-energy hopping in $(\mathbf{3})_2$ and $(\mathbf{5})_4$. Assuming that the number of energy-hopping sites (N) is 2 and 4, respectively, the experimental observables give the excitation-energy-hopping rates of 1.5 and 8.8 ps^{-1}, which are in a good agreement with the calculated Förster-type energy-transfer rates. In particular, in the case of $(\mathbf{5})_4$, the excitation-energy-hopping rate is faster than that of $(\mathbf{3})_2$ or previously reported assemblies because of the strong exciton coupling that results from the linear (J-type) orientation of transition dipole moments.

In conclusion, the strategy of this new square-type self-assembly system is considered to be an alternative method for increasing the energy-hopping efficiency in a self-assembled artificial light-harvesting apparatus. A further increase in the number of chromophores within this self-assembled system may result in a more efficient energy-hopping process with the ability to control its size. Our attempts to design new porphyrin assembly systems to test this possibility are currently underway.

Acknowledgements

The work at Kyoto was supported by Grants-in-Aid (no. 19205006 (A) and 20108001 "pi-Space") from MEXT. The work at Yonsei was financially supported by the Star Faculty and World Class University (no. 2008-8-1955) programs of the Ministry of Education, Science, and Technology of Korea and the AFSOR/AOARD grant (no. FA4869-08-1-4097). Research at Northwestern University was supported by the Chemical Sciences, Geosciences, and Biosciences Division, Office of Basic Energy Sciences, DOE under grant no. DE-FG02-99ER14999. C.M. thanks the JSPS fellowship for the young scientists. P.K., S.C., J.P., and J.M.L. acknowledge the fellowship of the BK21 program of the Ministry of Education, Science, and Technology of Korea.

[1] a) G. McDermott, S. M. Prince, A. A. Freer, A. M. Hawthornthwaite-Lawless, M. Z. Papiz, R. J. Cogdell, N. W. Isaacs, *Nature* **1995**, *374*, 517–521; b) A. W. Roszak, T. D. Howard, J. Southall, A. T. Gardiner, C. J. Law, N. W. Isaacs, R. J. Cogdell, *Science* **2003**, *302*, 1969–1972.

[2] a) M. R. Wasielewski, *Chem. Rev.* **1992**, *92*, 435–461; b) D. Gust, T. A. Moore, A. L. Moore, *Acc. Chem. Res.* **1993**, *26*, 198–205; c) D. Gust, T. A. Moore, A. L. Moore, *Acc. Chem. Res.* **2001**, *34*, 40–48; d) D. Holten, D. F. Bocian, J. S. Lindsey, *Acc. Chem. Res.* **2002**, *35*, 57–69; e) D. Kim, A. Osuka, *Acc. Chem. Res.* **2004**, *37*, 735–745.

[3] a) K. Sugiura, *Top. Curr. Chem.* **2003**, *228*, 65–85; b) Y. Nakamura, N. Aratani, A. Osuka, *Chem. Soc. Rev.* **2007**, *36*, 831–845.

[4] a) K. Sugiura, H. Tanaka, T. Matsumoto, T. Kawai, Y. Sakata, *Chem. Lett.* **1999**, 1193–1194; b) K. Sugiura, Y. Fujimoto, Y. Sakata, *Chem. Commun.* **2000**, 1105–1106; c) S. Rucareanu, O. Mongin, A. Schuwey, N. Hoyler, A. Gossauer, *J. Org. Chem.* **2001**, *66*, 4973–4988; d) M. Hoffmann, C. J. Wilson, B. Odell, H. L. Anderson, *Angew. Chem.* **2007**, *119*, 3183–3186; *Angew. Chem. Int. Ed.* **2007**, *46*, 3122–3125; e) M. Hoffmann, J. Kärnbratt, J. M.-H. Chang, L. M. Herz, B. Albinsson, H. L. Anderson, *Angew. Chem.* **2008**, *120*, 5071–5074; *Angew. Chem. Int. Ed.* **2008**, *47*, 4993–4996.

[5] a) X. Peng, N. Aratani, A. Takagi, T. Matsumoto, T. Kawai, I.-W. Hwang, T. K. Ahn, D. Kim, A. Osuka, *J. Am. Chem. Soc.* **2004**, *126*, 4468–4469; b) Y. Nakamura, I.-W. Hwang, N. Aratani, T. K. Ahn, D. M. Ko, A. Takagi, T. Kawai, T. Matsumoto, D. Kim, A. Osuka, *J. Am. Chem. Soc.* **2005**, *127*, 236–246; c) T. Hori, N. Aratani, A. Takagi, T. Matsumoto, T. Kawai, M.-C. Yoon, Z. S. Yoon, S. Cho, D. Kim, A. Osuka, *Chem. Eur. J.* **2006**, *12*, 1319–1327; d) T. Hori, X. Peng, N. Aratani, A. Takagi, T. Matsumoto, T. Kawai, Z. S. Yoon, M.-C. Yoon, J. Yang, D. Kim, A. Osuka, *Chem. Eur. J.* **2008**, *14*, 582–595.

[6] a) T. Imamura, K. Fukushima, *Coord. Chem. Rev.* **2000**, *198*, 133–156; b) J. Wojaczyński, L. Latos-Grażyński, *Coord. Chem. Rev.* **2000**, *204*, 113–171; c) S. Leininger, B. Olenyuk, P. J. Stang, *Chem. Rev.* **2000**, *100*, 853–908; d) E. Iengo, E. Zangrando, E. Alessio, *Eur. J. Inorg. Chem.* **2003**, 2371–2384; e) T. S. Balaban, *Acc. Chem. Res.* **2005**, *38*, 612–623; f) A. Satake, Y. Kobuke, *Tetrahedron* **2005**, *61*, 13–41; g) E. Iengo, E. Zangrando, E. Alessio, *Acc. Chem. Res.* **2006**, *39*, 841–851.

[7] a) C. M. Drain, J.-M. Lehn, *J. Chem. Soc. Chem. Commun.* **1994**, 2313–2315; b) C. A. Hunter, L. D. Sarson, *Angew. Chem.* **1994**, *106*, 2424–2426; *Angew. Chem. Int. Ed. Engl.* **1994**, *33*, 2313–2316; c) J. Wojaczyński, L. Latos-Grażyński, *Inorg. Chem.* **1995**, *34*, 1044–1053; d) J. Wojaczyński, L. Latos-Grażyński, M. M. Olmstead, A. L. Balch, *Inorg. Chem.* **1997**, *36*, 4548–4554; e) R. T. Stibrany, J. Vasudevan S. Knapp, J. A. Potenza, T. Emge, H. J. Schugar, *J. Am. Chem. Soc.* **1996**, *118*, 3980–3981; f) P. J. Stang, J. Fan, B. Olenyuk, *Chem. Commun.* **1997**, 1453–1454; g) R. V. Slone, J. T. Hupp, *Inorg. Chem.* **1997**, *36*, 5422–5423; h) C. M. Drain, F. Nifiatis, A. Vasenko, J. D. Batteas, *Angew. Chem.* **1998**, *110*, 2478–2481; *Angew. Chem. Int. Ed.* **1998**, *37*, 2344–2347; i) J. Fan, J. A. Whiteford, B. Olenyuk, M. D. Levin, P. J. Stang, E. B. Fleischer, *J. Am. Chem. Soc.* **1999**, *121*, 2741–2752; j) S. Bélanger, J. T. Hupp, *Angew. Chem.* **1999**, *111*, 2360–2362; *Angew. Chem. Int. Ed.* **1999**, *38*, 2222–2224; k) N. Fujita, K. Biradha, M. Fujita, S. Sakamoto, K. Yamaguchi, *Angew. Chem.* **2001**, *113*, 1768–1771; *Angew. Chem. Int. Ed.* **2001**, *40*, 1718–1721; l) M. L. Merlau, M. del Pilar Mejia, S. T. Nguyen, J. T. Hupp, *Angew. Chem.* **2001**, *113*, 4369–4372; *Angew. Chem. Int. Ed.* **2001**,

40, 4239–4242; m) E. Iengo, E. Zangrando, R. Minatel, E. Alessio, *J. Am. Chem. Soc.* **2002**, *124*, 1003–1013; n) G. A. Mines, B.-C. Tzeng, K. J. Stevenson, J. Li, J. T. Hupp, *Angew. Chem.* **2002**, *114*, 162–165; *Angew. Chem. Int. Ed.* **2002**, *41*, 154–157; o) A. Tsuda, S. Sakamoto, K. Yamaguchi, T. Aida, *J. Am. Chem. Soc.* **2003**, *125*, 15722–15723; p) M. Suzuki, K. Tsuge, Y. Sasaki, T. Imamura, *Chem. Lett.* **2003**, *32*, 564–565; q) M. Tominaga, K. Suzuki, M. Kawano, T. Kusukawa, T. Ozeki, S. Sakamoto, K. Yamaguchi, M. Fujita, *Angew. Chem.* **2004**, *116*, 5739–5743; *Angew. Chem. Int. Ed.* **2004**, *43*, 5621–5625; r) A. Tsuda, H. Hu, R. Tanaka, T. Aida, *Angew. Chem.* **2005**, *117*, 4962–4966; *Angew. Chem. Int. Ed.* **2005**, *44*, 4884–4888; s) A. Prodi, C. Chiorboli, F. Scandola, E. Iengo, E. Alessio, R. Dobrawa, F. Würthner, *J. Am. Chem. Soc.* **2005**, *127*, 1454–1462; t) R. A. Jensen, R. F. Kelley, S. J. Lee, M. R. Wasielewski, J. T. Hupp, D. M. Tiede, *Chem. Commun.* **2008**, 1886–1888.

[8] a) A. Tsuda, T. Nakamura, S. Sakamoto, K. Yamaguchi, A. Osuka, *Angew. Chem.* **2002**, *114*, 2941–2945; *Angew. Chem. Int. Ed.* **2002**, *41*, 2817–2821; b) I.-W. Hwang, T. Kamada, T. K. Ahn, D. M. Ko, T. Nakamura, A. Tsuda, A. Osuka, D. Kim, *J. Am. Chem. Soc.* **2004**, *126*, 16187–16198; c) T. Kamada, N. Aratani, T. Ikeda, N. Shibata, Y. Higuchi, A. Wakamiya, S. Yamaguchi, K. S. Kim, Z. S. Yoon, D. Kim, A. Osuka, *J. Am. Chem. Soc.* **2006**, *128*, 7670–7678; d) C. Maeda, T. Kamada, N. Aratani, T. Sasamori, N. Tokitoh, A. Osuka, *Chem. Eur. J.* **2009**, *15*, 9681–9684.

[9] a) Y. Kobuke, H. Miyaji, *J. Am. Chem. Soc.* **1994**, *116*, 4111–4112; b) K. Ogawa, Y. Kobuke, *Angew. Chem.* **2000**, *112*, 4236–4239; *Angew. Chem. Int. Ed.* **2000**, *39*, 4070–4073; c) K. Ogawa, T. Zhang, K. Yoshihara, Y. Kobuke, *J. Am. Chem. Soc.* **2002**, *124*, 22–23; d) R. Takahashi, Y. Kobuke, *J. Am. Chem. Soc.* **2003**, *125*, 2372–2373; e) Y. Kuramochi, A. Satake, Y. Kobuke, *J. Am. Chem. Soc.* **2004**, *126*, 8668–8669; f) O. Shoji, S. Okada, A. Satake, Y. Kobuke, *J. Am. Chem. Soc.* **2005**, *127*, 2201–2210; g) A. Satake, Y. Kobuke, *Org. Biomol. Chem.* **2007**, *5*, 1679–1691; h) J. E. Raymond, A. Bhaskar, T. Goodson III, N. Makiuchi, K. Ogawa, Y. Kobuke, *J. Am. Chem. Soc.* **2008**, *130*, 17212–17213.

[10] a) C. A. Hunter, J. K. M. Sanders, G. S. Beddard, S. Evans, *J. Chem. Soc. Chem. Commun.* **1989**, 1765–1767; b) S. Anderson, H. L. Anderson, J. K. M. Sanders, *Acc. Chem. Res.* **1993**, *26*, 469–475.

[11] a) C. Maeda, H. Shinokubo, A. Osuka, *Org. Lett.* **2007**, *9*, 2493–2496; b) C. Maeda, S. Yamaguchi, C. Ikeda, H. Shinokubo, A. Osuka, *Org. Lett.* **2008**, *10*, 549–553.

[12] Triazole-appended porphyrins were independently reported by Chen and Odobel: a) D.-M. Shen, C. Liu, Q.-Y. Chen, *Eur. J. Org. Chem.* **2007**, 1419–1422; b) M. Séverac, L. L. Pleux, A. Scarpaci, E. Blart, F. Odobel, *Tetrahedron Lett.* **2007**, *48*, 6518–6522.

[13] a) A. Osuka, H. Shimidzu, *Angew. Chem.* **1997**, *109*, 93–95; *Angew. Chem. Int. Ed. Engl.* **1997**, *36*, 135–137; b) N. Aratani, A. Osuka, Y. H. Kim, D. H. Jeong, D. Kim, *Angew. Chem.* **2000**, *112*, 1517–1521; *Angew. Chem. Int. Ed.* **2000**, *39*, 1458–1462; c) Y. H. Kim, D. H. Jeong, D. Kim, S. C. Jeoung, H. S. Cho, S. K. Kim, N. Aratani, A. Osuka, *J. Am. Chem. Soc.* **2001**, *123*, 76–86.

[14] a) N. Miyaura, A. Suzuki, *Chem. Rev.* **1995**, *95*, 2457–2483; b) N. Aratani, A. Osuka, *Org. Lett.* **2001**, *3*, 4213–4216; c) Y. Nakamura, S. Y. Jang, T. Tanaka, N. Aratani, J. M. Lim, K. S. Kim, D. Kim, A. Osuka, *Chem. Eur. J.* **2008**, *14*, 8279–8289.

[15] a) O. Glatter, *Neutron, X-ray, and Light Scattering*, Elsevier, Amsterdam, **1991**, pp. 33–82; b) A. Guinier, G. Fournet, *Small Angle Scattering*, Wiley, New York, **1955**.

[16] D. I. Svergun, M. H. Koch, *Rep. Prog. Phys.* **2003**, *66*, 1735–1782.

[17] D. I. Svergun, *J. Appl. Crystallogr.* **1992**, *25*, 495–503.

[18] a) D. M. Tiede, R. Zhang, L. X. Chen, L. Yu, J. S. Lindsey, *J. Am. Chem. Soc.* **2004**, *126*, 14054–14062; b) S. J. Lee, K. L. Mulfort, J. L. O'Donnell, X. Zuo, A. J. Goshe, P. J. Wesson, S. T. Nguyen, J. T. Hupp, D. M. Tiede, *Chem. Commun.* **2006**, 4581–4583.

[19] W. J. Hehre, *A Guide to Molecular Mechanics and Quantum Chemical Calculations*, Wavefunction, Irvine, **2003**.

[20] a) G. Trinkunas, J. L. Herek, T. Polivka, V. Sundström, T. Pullerits, *Phys. Rev. Lett.* **2001**, *86*, 4167–4170; b) G. Trinkunas, *J. Lumin.* **2003**, *102*, 532–535.

[21] a) S. E. Bradforth, R. Jimenez, F. van Mourik, R. van Grondelle, G. R. Fleming, *J. Phys. Chem.* **1995**, *99*, 16179–16191; b) R. Jimenez, S. N. Dikshit, S. E. Bradforth, G. R. Fleming, *J. Phys. Chem.* **1996**, *100*, 6825–6834.

[22] a) M. Kasha, *Radiat. Res.* **1963**, *20*, 55–71; b) M. Kasha, H. R. Rawls, M. A. EL-Bayoumi, *Pure Appl. Chem.* **1965**, *11*, 371–392; c) G. D. Scholes, K. P. Ghiggino, *J. Phys. Chem.* **1994**, *98*, 4580–4590.

[23] J. R. Lakowicz, *Principles of Fluorescence Spectroscopy*, Springer, Heidelberg, **2006**.

[24] Förster paper: a) S. E. Bradforth, R. Jimenez, F. van Mourik, R. van Grondelle, G. R. Fleming, *J. Phys. Chem.* **1995**, *99*, 16179–16191; b) I.-W. Hwang, D. M. Ko, T. K. Ahn, Z. S. Yoon, D. Kim, X. Peng, N. Aratani, A. Osuka, *J. Phys. Chem. B* **2005**, *109*, 8643–8651; c) I.-W. Hwang, M. Park, T. K. Ahn, Z. S. Yoon, D. M. Ko, D. Kim, F. Ito, Y. Ishibashi, S. R. Khan, Y. Nagasawa, H. Miyasaka, C. Ikeda, R. Takahashi, K. Ogawa, A. Satake, Y. Kobuke, *Chem. Eur. J.* **2005**, *11*, 3753–3761; d) I.-W. Hwang, Z. S. Yoon, J. Kim, T. Kamada, T. K. Ahn, N. Aratani, A. Osuka, D. Kim, *J. Photochem. Photobiol. A* **2006**, *178*, 130–139; e) R. F. Kelley, S. J. Lee, T. M. Wilson, Y. Nakamura, D. M. Tiede, A. Osuka, J. T. Hupp, M. R. Wasielewski, *J. Am. Chem. Soc.* **2008**, *130*, 4277–4284.

Received: November 21, 2009
Published online: March 26, 2010

